Published in "Colloids and Surfaces A: Physicochem. Eng. Aspects" 250 (2004) 325–336

Oil-continuous microemulsions mixed with an amphiphilic graft copolymer or with the parent homopolymer
Polymer–droplet interactions as revealed by phase behavior and light scattering

Anna Holmberg[a], Lennart Piculell[a,*], Peter Schurtenberger[b], Ulf Olsson[a]

[a] *Physical Chemistry 1, Center for Chemistry and Chemical Engineering, University of Lund, P.O. Box 124, SE-22100 Lund, Sweden*
[b] *Soft Condensed Matter Group, Physics Department, University of Fribourg, Perolles, CH-1700 Fribourg, Switzerland*

Received 19 January 2004; accepted 15 June 2004
Available online 18 September 2004

Abstract

Polymer–droplet interactions have been studied in AOT/water/isooctane oil-continuous microemulsions mixed with an amphiphilic graft copolymer, or with the parent homopolymer (AOT = sodium bis(2-ethylhexyl) sulfosuccinate). The graft copolymer has an oil-soluble poly(dodecyl methacrylate) backbone and water-soluble poly(ethylene glycol) side chains. Pseudo-ternary polymer/droplet/isooctane phase diagrams have been established for both the parent homopolymer and the graft copolymer, and the two types of mixture display entirely different phase behavior. The homopolymer–droplet interaction is repulsive, and a segregative phase separation occurs at high droplet concentrations. By contrast, the graft copolymer–droplet interaction is attractive: the polymer is insoluble in the pure oil, but dissolves in the microemulsion. A comparatively high concentration of droplets is required to solubilize even small amounts of polymer. Static and dynamic light scattering has been performed in order to obtain information on structure and dynamics in the two types of mixture. For optically matched microemulsions, with a vanishing excess polarizability of the droplets, the polymer dominates the intensity of scattered light. The absolute intensity of scattered light increases as phase separation is approached owing to large-scale concentration fluctuations. Dynamic light scattering shows two populations of diffusion coefficients; one population originates from “free” microemulsion droplets and the other from the polymer (for homopolymer mixtures) or from polymer–droplet aggregates (for mixtures with the graft copolymer). The graft copolymer forms large polymer–droplet aggregates with a broad size distribution, which coexist with a significant fraction of free droplets.

Keywords: Amphiphilic polymer; Microemulsion; Polymer–surfactant interactions; Phase behavior; Light scattering

1. Introduction

Liquid mixtures of amphiphilic polymers with organized surfactant solutions are widely studied, because of their importance in various industrial applications. The introduction of hydrophobic moieties on a hydrophilic polymer or vice versa, typically have dramatic effects on the miscibility of the polymer with the surfactant solution, and on the rheology of the resulting mixture [1,2].

We have previously synthesized a novel amphiphilic graft copolymer by grafting PEO side chains, with a weight average molar mass of 2000 g/mol, onto a hydrophobic poly(dodecyl methacrylate) (PDMA) backbone (Fig. 1) [3]. The side chains are water-soluble and the backbone is soluble in oils, such as isooctane or cyclohexane. The PDMA-g-PEO graft copolymer is not soluble in oil nor in water, but it is quite soluble in oil-continuous microemulsions based on the anionic surfactant AOT (AOT = sodium bis(2-ethylhexyl) sulfosuccinate). Such microemulsions are thermodynamically stable solutions of spherical AOT-coated water droplets in oil [4]. The stable microemulsion phase extends to large vol-

* Corresponding author. Tel.: +46 46 2229518; fax: +46 46 2224413.
E-mail address: lennart.piculell@fkem1.lu.se (L. Piculell).

0927-7757
doi:10.1016/j.colsurfa.2004.06.040

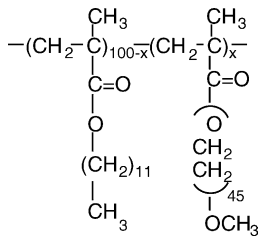

Fig. 1. Structure of hydrophobically modified poly(dodecyl methacrylate). *x* is the number of PEO chains per 100 monomers.

ume fractions of droplets (typically 70%), and the droplet size is conveniently controlled by the water-to-surfactant ratio. In a series of studies, we have showed that the PDMA-g-PEO graft copolymer can give rise to a dramatic increase in the viscosity when added to AOT/water/cyclohexane oil-continuous microemulsions [3,5,6]. Analogous viscosifying effects of structurally simpler amphiphilic triblock copolymers have been found and studied in detail, primarily by Eicke's group [7–10]. The relative viscosity increase of added PDMA-g-PEO graft copolymer was found to depend on a number of factors, such as the concentration and the degree of substitution of the copolymer and the size and concentration of the droplets. At sufficiently high-polymer concentrations, a maximum in the viscosity was obtained when the droplet concentration was increased progressively at a constant polymer concentration [5]. Thus, these oil-continuous systems display many similarities with the analogous, but more familiar, water-continuous mixtures, where micelle-forming surfactants are mixed with hydrophobically modified water-soluble graft copolymers [11–28].

Results from PFG-NMR measurements on PDMA-g-PEO/microemulsion mixtures showed a good correlation between the polymer self-diffusion and the macroscopic viscosity of the system: systems with high viscosity displayed slow polymer diffusion, and vice versa [6]. The enhancement of the viscosity and decrease of the diffusion could thus be attributed to the formation of polymer–droplet aggregates, where the polymer backbone is dissolved in the oil-continuous phase and the side chains are anchored into the water droplets. However, the same study also showed that the droplet self-diffusion was always much faster than the polymer diffusion. This was interpreted in terms of a considerable fraction (30–60%) of free droplets, i.e., droplets not bound in polymer–droplet aggregates.

The unsubsituted PDMA polymer is soluble in the microemulsions over a large composition range, but it was found to cause phase separation into two clear liquid phases at high droplet concentrations [6]. Another type of phase separation was encountered in mixtures with the graft copolymer. As expected, mixtures at a constant polymer concentration eventually separate at sufficiently low droplet concentrations (we recall that the graft copolymer is not soluble in pure oil). However, a phase separation was also encountered on dilution with oil at a constant polymer/droplet ratio. The latter effect was explained in terms of a decrease in the number of bound droplets per polymer, attributable to an increasing entropic cost of binding droplets on dilution with oil. At some stage, the number of bound droplets per polymer went below the minimum value compatible with solubility.

In this work, we present new results elucidating the effects of PEO grafts on the interactions between PDMA molecules and microemulsion droplets. To this end we make detailed comparisons of microemulsions containing either unsubstituted PDMA or the PDMA-g-PEO graft copolymer. We map out the macroscopic phase behavior of the respective pseudoternary polymer/droplet/oil mixtures (at two different droplet sizes), and we find that the presence or absence of the PEO grafts changes the phase behavior entirely. We also report detailed studies of a range of single-phase mixtures, using both static and dynamic light scattering, again finding large differences between the two types of polymer.

In this work, we have used isooctane, rather than cyclohexane, as the oil. This change of oil, compared to our previous studies, was made for the following reasons. First, the microemulsion phase is extended to larger droplets with isooctane (otherwise, the two ternary AOT/water/oil phase diagrams are similar). Our previous studies have shown that at constant volume fractions of droplets, many of the effects of added polymer become stronger for larger droplets. Although, no quantitative viscosity measurements are reported here, we have confirmed that the strongly viscosifying effect of the graft copolymer occurs also in the microemulsions with isooctane.

The second, very important, advantage of using isooctane in the present study is technical. In the light scattering studies, we wanted to take advantage of the so-called "optical matching" between the surfactant-covered water droplets and the oil. At a certain surfactant/water ratio (i.e., for a certain droplet size), a droplet in the microemulsion happens to have the same average refractive index as the oil. In the vicinity of this match point the droplet scattering is strongly suppressed, as has been shown in previous studies [29,30]. Under these conditions, the scattering from other dissolved objects (polymer molecules, in the present case) may dominate, even if the dissolved molecules are grossly outnumbered by the water droplets. Contrast variation experiments have been used successfully to study the effects of other additives, such as enzymes and water-soluble polymers, in AOT/water/isooctane microemulsions [30,31]. As it turns out, the match point in AOT/water/oil microemulsions occurs at a larger droplet size for isooctane than for cyclohexane. As explained earlier, the larger droplet sizes are more interesting in the present context.

2. Experimental

2.1. Chemicals

Dodecyl methacrylate (DMA) monomers were purified by passing through a column of basic alumina (BDH, active basic, Brockman Grade 1). The chemicals

2,2′-azobisisobutyronitrile (AIBN, Merck, 97%), potassium methylate (Merck, 97%), isobutyric acid (BDH, 99%), toluene (p.a.), poly(ethylene glycol) monomethyl ether (MPEO; M_n = 2000, Aldrich-Chemie), AOT (Sigma, 99%), and isooctane (Fluka, 99.5%) were used as delivered. The hygroscopic AOT was stored in a desiccator. Millipore water was used in the microemulsions.

2.2. Polymer synthesis

The synthesis of the graft copolymer (Fig. 1) has been described in detail [3], and only a brief description is given here. Poly(dodecyl methacrylate) was synthesized by radical polymerisation of DMA in toluene with AIBN as the initiator. The polymer was purified by repeated precipitation from toluene/methanol and was subsequently dried in vacuum.

Monofunctional MPEO was grafted onto PDMA as described by Wesslén et al. [32]. Potassium methylate was added to a toluene solution of MPEO. The mixture was refluxed and methanol was distilled off. The MPEO-alkoxide solution was mixed with a toluene solution of PDMA. The solution was refluxed under nitrogen. Since, the grafting was carried out in dilute homogeneous solution the grafts may be assumed to be randomly distributed along the backbone [33]. The reaction was stopped by neutralizing the reaction mixture with isobutyric acid. The crude polymer was reprecipitated twice from toluene/diethyl ether, dried, redissolved in tetrahydrofuran (THF), and precipitated by addition of water. The solution was poured into a dialysis bag and dialyzed against water to remove unreacted MPEO.

2.3. Polymer characterization

The unsubstituted PDMA (P_0) and the graft copolymer (P_2) used in this study were the same batches as in one of our previous studies, where details on the methods of characterization are also given [6]. The results for P_0 are collected in Table 1. The graft copolymer P_2 was made by grafting PEO side chains onto P_0. NMR experiments showed the grafting density to be 2.4 PEO side chains per 100 repeating units of the backbone [6]. No data on P_2 are given in Table 1, since our previous study showed that the graft co-polymer self-associates slightly in the solvent (THF) [6]. Thus, the average molar mass of P_2 obtained in THF does not reflect singly dispersed molecules.

Table 1
Characteristics of the unsubstituted polymer P_0

Solvent	M_w (g/mol)	M_w/M_n	r_h (nm)	r_g (nm)	c^* (g/dm^3)
THF	370000	1.9[a]	–	16[a]	–
Isooctane	300000	–	14[b], 12[c]	24[b]	31[c]
Cyclohexane	–	–	14[c]		21[c]

[a] From GPC/light scattering; [6].
[b] From light scattering; this work.
[c] From intrinsic viscosity.

The intrinsic viscosity of P_0 in isooctane was determined at 20 °C with an Ubbelohde Capillary Viscometer (Schott Geräte, 0.46 mm capillary diameter). The sample concentration range was 2–16 g/dm^3. The intrinsic viscosity $[\eta]$ = 0.032 dm^3/g for P_0 in isooctane yields a hydrodynamic radius of 12 nm and an overlap concentration $c^* \approx 31$ g/dm^3. The corresponding values for P_0 in cyclohexane were found[3] to be $[\eta]$ = 0.048 dm^3/g and $c^* \approx 21$ g/dm^3, indicating that cyclohexane is a better solvent than isooctane for PDMA.

For easy reference, Table 1 also gives the values of the weight average molar mass, M_w, the radius of gyration, r_g, and the hydrodynamic radius, r_h, of P_0 in isooctane obtained by light scattering, as described below.

2.4. Sample preparation

Oil-continuous microemulsions of AOT/water/isooctane were prepared at selected compositions, and the desired amount of polymer P_0 or P_2 was added. All samples used for light scattering experiments were transparent and homogeneous. The samples were transferred into cylindrical tubes with a Teflon plug, which were centrifuged 30 min at approximately 6000 × g and 25 °C in order to remove dust particles from the scattering volume. Phase diagrams at fixed droplet sizes were determined by preparing initially biphasic (for P_0) or monophasic (for P_2) samples. Biphasic samples were recognized by their turbidity immediately after mixing, whereas monophasic samples were clear. The samples were diluted successively with oil until they became clear (for P_0) or turbid (for P_2). Compositions corresponding to transitions between clear and turbid samples (cloud points) were used to construct the phase boundaries.

2.5. Light scattering measurements

Static (SLS) and dynamic (DLS) light scattering was performed with an ALV-5000 spectrophotometer equipped with an argon-laser (Coherent, model Innova 300, λ = 488 nm), a digital autocorrelator (ALV) and variable angle detection system. Measurements were made at 25.0 ± 0.1 °C.

The refractive index increment (dn/dc) of polymer P_0 in isooctane was determined, using a temperature-controlled interferometric refractometer from Wyatt/Optilab, working at λ = 488 nm. The change in refractive index dn was measured and dn/dc calculated to 0.1225 ± 0.0012 ml/g at 25 °C.

SLS measurements were performed at 26 different angles ($15^\circ \le \theta \le 140^\circ$) and approximately 10 individual measurements were averaged for each angle, thus yielding the scattering intensity $\langle I(\theta)\rangle$. For each value of θ, the data were corrected for solvent scattering and normalized by using toluene as a reference standard:

$$\Delta\langle I(\theta)\rangle_n = \frac{\langle I(\theta)\rangle - \langle I_s(\theta)\rangle}{\langle I_{tol}(\theta)\rangle} \quad (1)$$

here $\langle I_s(\theta)\rangle$ is the solvent intensity and $\langle I_{tol}(\theta)\rangle$ the intensity of toluene. The data were converted into absolute scattering

intensities ("excess Rayleigh ratios") ΔR_θ using:

$$\Delta R_\theta = \Delta\langle I(\theta)\rangle_n R_{\text{tol}}(\theta)\left(\frac{n}{n_{\text{tol}}}\right)^2 \quad (2)$$

here $R_{\text{tol}}(\theta)$ = 39.6 × 10^{-4} m^{-1} is the Rayleigh ratio of toluene, n the refractive index of the solution and n_{tol} (= 1.499) the refractive index of toluene [34]. Since, the measurements were performed close to the optical match point (see below) we have put n_0 equal to the refractive index of isooctane.

The intensity scattered from a dilute solution of large interacting macromolecules is expressed by the Debye equation [35].

$$\frac{Kc}{\Delta R_\theta} = \frac{1}{P(\theta)}\left(\frac{1}{M_{\text{W}}} + 2Bc + \cdots\right) \quad (3)$$

here M_{w} is the weight-average molar mass and B the second virial coefficient. K is an optical constant equal to $4\pi^2 n_o{}^2(\text{d}n/\text{d}c)^2/\lambda^4 N_{\text{A}}$, where λ is the wavelength of the incident light in vacuum, dn/dc the refractive index increment and N_{A} Avogadro's constant. $P(\theta)$ is the form factor, which may be expressed as:

$$\frac{1}{P(\theta)} = 1 + \frac{r_{\text{g}}^2}{3}q^2 \quad (4)$$

where q is the magnitude of the scattering vector, equal to $4\pi n/\lambda \sin(\theta/2)$, and r_{g} is the radius of gyration. M_{w} for the homopolymer in isooctane was obtained from the concentration dependence of $Kc/\Delta R_\theta$ by extrapolating to zero angle. The mean square radius of gyration of a polymer or a polymer–droplet aggregate (as appropriate) was obtained from the intercept and the slope of $1/\Delta R_\theta$ versus q^2 using

$$\frac{1}{\Delta R_\theta} = \frac{1}{\Delta R_0}\left(1 + \frac{r_{\text{g}}^2}{3}q^2\right) \quad (5)$$

where ΔR_0 is the absolute intensity at $q = 0$.

DLS measurements were performed at the scattering angles 30° or 45° for pure microemulsion samples, at three different angles (30° ≤ θ ≤ 90°) for samples with polymer P_0, and at eight different angles (30° ≤ θ ≤ 135°) for samples with polymer P_2. At least five measurements of duration of 1–10 min were performed for each sample. The individual correlation functions were analyzed, using a second-order cumulant fit.[36] In the cumulant fit, the autocorrelation function is expanded about a mean initial decay rate or characteristic line width $\langle\Gamma\rangle$, as a polynomial in the sample time with cumulants as parameters to be fitted. A z-average collective diffusion coefficient D can be calculated from $\langle\Gamma\rangle$ using the relation:

$$D = \frac{\langle\Gamma\rangle}{q^2} \quad (6)$$

Polymer-containing samples showed an angular dependence of the scattered intensity. The z-average collective diffusion coefficients, D, were then obtained from slopes of $\langle\Gamma\rangle$ plotted versus the scattering vector q^2. Linear plots passing through the origin were obtained for all polymer-containing samples indicating a diffusive process.

At infinite dilution and at q = 0 (if there is an angular dependence of the scattering intensity) the z-average collective diffusion coefficient D equals the self-diffusion coefficient, D_0. A z-averaged hydrodynamic radius r_{h} can be calculated from D_0, using the Stokes–Einstein relation

$$r_{\text{h}} = \frac{kT}{6\pi\eta_0 D_0} \quad (7)$$

where k is the Boltzmann constant, T the absolute temperature and η_0 the solvent viscosity. An apparent z-averaged hydrodynamic radius $r_{\text{h}}^{\text{app}}$ is obtained if D at a finite concentration is used in Eq. (7).

The DLS data were also analyzed with the CONTIN method to obtain the inverse Laplace transformation of the autocorrelation function and the distribution of decay times Γ [37]. The CONTIN data were converted into intensity weighted distributions of diffusion coefficients.

2.6. Light scattering from microemulsion droplets

For the spherical water-in-oil droplets obtained with AOT as the surfactant, the water core radius, r_{w}, increases linearly with the molar ratio of water to surfactant, w_0, by the relation

$$r_{\text{w}} = \frac{3w_0 v_{\text{w}}}{a_{\text{AOT}}} \quad (8)$$

where v_{w} is the molecular volume of water and a_{AOT} is the headgroup area of AOT (= 57 Å^2 in isooctane [38]). The total average intensity of scattered light $\langle I\rangle$ from a polydisperse solution of microemulsion particles is given by [39]:

$$\langle I\rangle \propto \frac{\langle\alpha^2\rangle\phi_{\text{d}}}{\lambda^4\langle V\rangle}S(0) \quad \text{and} \quad \langle\alpha^2\rangle \propto \int f(r)\alpha^2(r)\text{d}r \quad (9)$$

where $\langle V\rangle$ is the average volume, $\langle\alpha^2\rangle$ the mean square excess polarizability and $f(r)$ the size distribution function for the microemulsion droplets. In the coated sphere model, the polarizability of a droplet is given by [38]:

$$\alpha = 4\pi\varepsilon_0\left[\left(\frac{\varepsilon_{\text{w}} - \varepsilon_{\text{o}}}{\varepsilon_{\text{w}} + 2\varepsilon_{\text{o}}}r_{\text{w}}^3\right) + \left(\frac{\varepsilon_{\text{s}} - \varepsilon_{\text{o}}}{\varepsilon_{\text{s}} + 2\varepsilon_{\text{o}}}3\delta r_{\text{w}}^2\right)\right] \quad (10)$$

where ε_{s}, ε_{w} ,and ε_{o} are the optical dielectric constants ($\varepsilon_i = n_i{}^2$ where n_i is the refractive index) of surfactant, water and oil, respectively, and δ corresponds to the surfactant layer thickness ($\delta = v_{\text{s}}/a_{\text{s}}$ for $r_{\text{w}} \gg \delta$). The optical dielectric constants are ε_{s} = 2.205 for AOT, ε_{w} = 1.795 for water and ε_{o} = 1.942 for isooctane [30]. Since, $\varepsilon_{\text{w}} < \varepsilon_{\text{o}}$ and $\varepsilon_{\text{s}} > \varepsilon_{\text{o}}$, α vanishes at some specific value of w_0. This w_0 value is called the optical match point and was first encountered by Zulauf and Eicke, who analyzed the dependence of the scattered intensity on the water-to-surfactant molar ratio for AOT/water/isooctane microemulsions in terms of a simple core-shell model for the droplets [29]. Experimentally, one

observes a finite, but well-defined, minimum of the intensity versus w_0, and a sigmoidal shape of r_h versus w_0 around this minimum of the intensity. The latter features have been explained by droplet polydispersity, which leads to an incomplete matching and a non-zero value of the intensity at the optical match point [29]. The existence of an optical match point makes it possible to perform optical contrast variation experiments.

The location of the optical match point can be shifted by changing the solvent in the microemulsion because of the strong dependence of α on the dielectric constant ε_o [30,38]. Thus, the optical match point occurs at larger droplets (around w_0 = 30) for isooctane than for cyclohexane (around w_0 = 10), as was already pointed out in the Introduction. The optical match point can also be shifted by additives. Polymer P_0 is oil-soluble and big compared to the water core radius (three to four times bigger than r_w). The optical matching should not be altered by the addition of P_0 provided that the composition of the droplets stays unchanged. When polymer P_2 is added the PEO side chains will be dissolved inside the water droplets. This will change the polarizability of the microemulsion. We have calculated the polarizability of AOT/water/isooctane oil-continuous microemulsions with and without PEO, and the insertion of 1 PEO side chain per droplet resulted in a quite minor shift of the optical match point towards higher w_0. From this we may assume that the optical properties of the polymer-bound droplets are not dramatically different from those of the free droplets, at a given microemulsion composition.

3. Results and discussion

3.1. Phase behavior

In our previous studies, we have taken the ternary microemulsion phase diagram as our point of departure when describing the phase behavior of microemulsions mixed with either unsubstituted PDMA or the graft copolymer: We have seen how the microemulsion phase behavior is modified in the presence of the respective polymers [3,5,6]. In the present study, we take an alternative approach, where we view the microemulsion droplet (at a constant size) as a pseudo-component in the mixture. Ternary polymer/droplet/oil phase diagrams can then be established for various constant droplet sizes, i.e., constant w_0 values. Fig. 2 shows such diagrams for mixtures of P_0 or P_2 with the two extreme droplet sizes investigated in the present study. The diagrams are partial; data are given mainly for comparatively low polymer concentrations. We have previously found that it takes a very long time to prepare homogeneous mixtures of P_2 with microemulsions at polymer concentrations exceeding a few weight percent [3,6]. In addition, scarcity of material precluded detailed investigations of systems with very high polymer concentrations. Note that, in the concentration range shown, the pseudo-binary droplet–oil mixture is well within the microemulsion region, which extends to ca. 70% droplets [4].

The phase diagrams in Fig. 2 show that the effects on the microemulsions are quite different for unsubstituted PDMA and for the graft copolymer. Fig. 2a shows that P_0 is miscible with the droplets in the dilute concentration range, but at higher concentrations a phase separation into two clear liquid phases occurs. The phase compositions were not determined, again because of scarcity of material, but the phase bound-

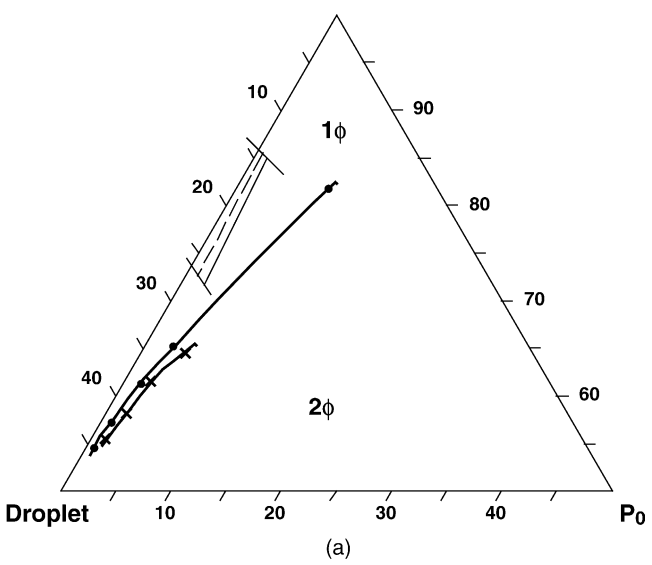

(a)

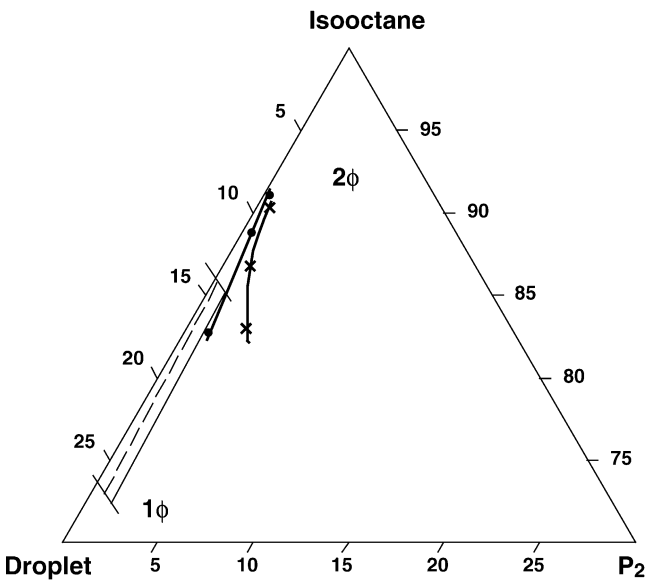

(b)

Fig. 2. Partial pseudo-ternary phase diagrams of (a) P_0/droplet/isooctane and (b) P_2/droplet/isooctane. Concentrations are in given weight percent; note the different scales in (a) and (b). The fat solid lines indicate phase boundaries between one-phase areas, 1ϕ, and two-phase areas, 2ϕ, for w_0 = 22.5 (crosses) and w_0 = 37.5 (dots). The thin solid (for w_0 = 22.5) and dashed (for w_0 = 37.5) lines show the composition ranges of the polymer-containing microemulsions investigated by light scattering.

aries have the characteristic features of a segregative phase separation into one polymer-rich phase and one droplet-rich phase. Similar phase diagrams have previously been established for aqueous mixtures of polymers and surfactant micelles [40,41]. In analogy with the aqueous micelle/polymer segregation [41], the P_0/droplet segregation in Fig. 2a is stronger for larger droplets. On standing, the biphasic mixtures separated into two clear phases. The polymer-rich top phase had a low viscosity, indicating that this was the more dilute phase. This is expected for flexible polymers, which have a higher osmotic pressure (on a weight basis) than compact particles, and is again in agreement with the findings for the analogous aqueous polymer/micelle mixtures [40,41].

An entirely different phase behavior is found for mixtures of the graft copolymer with droplets in oil; see Fig. 2b. As already pointed out, the graft polymer is not oil-soluble. Therefore, a two-phase area extends from the isooctane–P_2-axis. Fig. 2b shows that this area dominates the dilute part of the phase diagram (<10 wt.% droplets), where it extends almost all the way to the isooctane–droplet axis. Here, a very low concentration of the copolymer suffices to cause phase separation. Expressed alternatively, a large concentration of water droplets is required to solubilize even small amounts of polymer. At larger droplet concentrations, the one-phase area increases, but it is nevertheless, clear that the region of P_2/droplet miscibility is limited to a rather narrow region of the phase diagram, where the weight fraction of droplets is quite large, and much larger than that of the polymer.

Another feature shown by Fig. 2b is that the weight fraction of droplets required to solubilize the polymer increases with increasing droplet size. A more microscopic view of the requirements for miscibility is presented in Fig. 3. Here we show the two phase boundaries of Fig. 2b expressed in terms of the number concentrations of droplets ($c_{droplets}$) and of polymer side chains (c_{PEO}), assuming that the droplet/side chain ratio is of particular significance for the solubility.

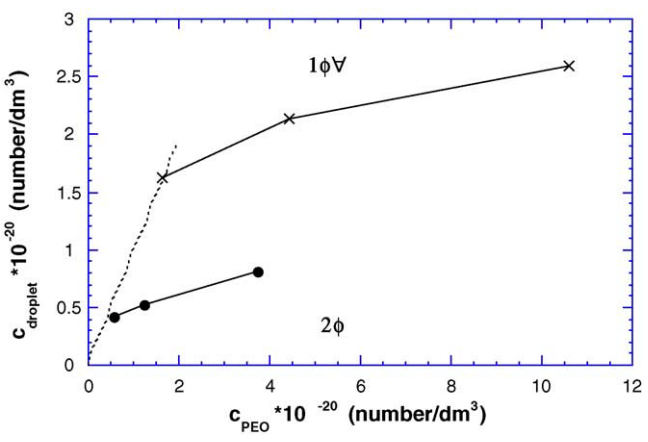

Fig. 3. Number concentration of droplets vs. number concentration of PEO side chains in mixtures of P_2/droplets/isooctane at the phase boundary between the one phase area, 1ϕ, and the two-phase area, 2ϕ, for w_0 = 22.5 (crosses) and w_0 = 37.5 (circles). The dotted line indicates a ratio of 1 PEO side chain per droplet.

(The number concentration of copolymer molecules may be obtained by dividing c_{PEO} by 49, the average number of side chains per polymer molecule.) From Fig. 3, we see that the number concentration of droplets required to dissolve a given concentration of the graft copolymer is lower for larger droplets, as might be expected.

Fig. 3 shows more clearly another feature evident from Fig. 2b, i.e., that the droplet concentration required to dissolve a certain polymer concentration increases sharply at low polymer contents, and then much more slowly at higher polymer concentrations. This means that the overall side chain/droplet ratio at dissolution varies over the range shown, from roughly one at the lowest polymer concentrations to five at the highest polymer concentrations. It is important to realize, however, that this overall ratio does not reflect the actual stoichiometry of the complex. Our previous study by NMR self-diffusion, demonstrated that there is always a large fraction of free droplets in the mixtures [6]. (This finding is given further support by the light scattering studies presented below.) Thus, the number of side chains per bound droplet at a given composition is higher than the overall ratio that may be extracted from Fig. 3. The previous NMR studies also showed that the side chain-bound droplet ratio increases quite rapidly on dilution; bound droplets leave the polymer on dilution for entropic reasons. This, we believe, is the reason for the curvature of the phase boundaries in Figs. 2b and 3: at a given overall side chain/droplet ratio, a larger fraction of the droplets will be polymer-bound, thus maintaining polymer solubility, when the overall concentration increases.

The graft copolymer/droplet/oil phase diagram (Figs. 2b and 3) bears an interesting resemblance to that obtained for certain “reverse” mixtures of an amphiphilic water-soluble polymer (e.g., a hydrophobically modified polymer or a protein) with a micelle-forming surfactant in water [42–44]. In the latter cases, added surfactant first leads to a phase-separation of an insoluble Polymer–surfactant complex, but this is followed by a re-dissolution at still higher surfactant contents, where a higher degree of surfactant binding makes the complex again soluble. The redissolved complexes typically contain micelle-like surfactant aggregates that solubilize the hydrophobic moieties of the amphiphilic polymer, and a higher concentration of the amphiphilic polymer requires a higher surfactant concentration for total solubilization. Similarly, in the graft copolymer/droplet/oil mixtures of the present study, an increasing concentration of surfactant-covered water droplets is required to solubilize the hydrophilic side chains of the graft copolymer as the polymer concentration is increased.

3.2. Light scattering: strategy

Static and dynamic light scattering was performed in order to obtain information on structure and dynamics (and, indirectly, on interactions) in oil-continuous microemulsions, containing either the unsubstituted PDMA or the graft

Table 2
Characteristics of the most concentrated (ϕ_d = 0.20) microemulsions used in the light scattering experiments

w_0	AOT (wt.%)	Water (wt.%)	r_w (nm)	$c_{droplets}$ (nr/dm^3)
22.5	13.8	12.6	3.6	5.34×10^{20}
25.0	13.1	13.3	4.0	4.09×10^{20}
27.5	12.5	13.9	4.3	3.23×10^{20}
30.0	11.9	14.5	4.7	2.59×10^{20}
32.5	11.4	15.0	5.1	2.10×10^{20}
35.0	10.9	15.5	5.5	1.73×10^{20}
37.5	10.5	15.9	5.9	1.45×10^{20}

copolymer. Mixtures of interest are monophasic samples, including such compositions that give high viscosities for the graft copolymer. Such samples are characterized by a weight fraction of droplets that is much larger than that of the polymer (see the position of the one-phase area in Fig. 2b). By using microemulsions with a composition close to the optical match point (at w_0 = 30), we may hope to nevertheless, suppress the droplet scattering and find conditions where the polymer dominates the intensity of scattered light. However, some droplet scattering will still remain (see above), giving useful information especially in the DLS experiments.

We chose to study a matrix of samples based on seven different droplet sizes, centered around the match point, which were prepared at a set of fixed volume concentrations of droplets. Thus, for the polymer-free microemulsions, samples were made for all the seven droplet sizes at ϕ_d equal to 0.20, 0.15, 0.10 and 0.05. The sample compositions for the largest droplet concentration are specified in Table 2.

In all P_2-containing samples, the overall ratio between the number of polymer molecules and the number of droplets was kept constant, corresponding to 1 PEO side chain per droplet. For each mixture with the copolymer, a reference mixture was also made that contained P_0 instead of P_2, but at the same weight concentration. Since, the number of droplets decreases with increasing droplet size at a fixed ϕ_d, the polymer concentration decreases accordingly in our mixtures, as shown in Table 3. Table 3 shows that the sample matrix with polymer includes, samples at ϕ_d ranging from 0.10 to 0.20. The composition ranges of the polymer-containing microemulsions were chosen so that all mixtures were monophasic (see the phase diagrams in Fig. 2, where these composition ranges are indicated for the largest and smallest droplet sizes). Finally, solutions of polymer P_0 in isooctane were also prepared at four different concentrations: 10.0, 7.50, 5.00 and 2.50 g/dm^3. In all polymer-containing samples, the polymer concentration was kept below the overlap concentration of P_0 (31 g/dm^3; Table 1).

Table 3
Compositions of polymer-containing microemulsions used in the light scattering experiments

w_0	c_{pol} (g/dm^3)			
	ϕ_d = 0.20	ϕ_d = 0.17	ϕ_d = 0.13	ϕ_d = 0.10
22.5	11.1	9.2	7.3	5.5
25.0	8.8	7.4	5.9	4.4
27.5	7.3	6.1	4.8	3.7
30.0	6.0	5.0	4.0	3.0
32.5	5.0	4.2	3.3	2.5
35.0	4.2	3.5	2.8	2.1
37.5	3.6	3.0	2.4	1.8

In the following, we will first present the light scattering results for the two reference systems, i.e., polymer-free microemulsions and solutions of the unsubstituted PDMA in isooctane. Then follow the results from the polymer-containing microemulsions, which are divided into two separate sections, dealing with SLS and DLS, respectively.

3.3. Light scattering from pure microemulsions

Our light scattering results from the pure microemulsions reproduce those reported by previous authors on the same system [29,30]. The SLS results are summarized in Fig. 4. The absolute intensity ΔR_0, i.e., the excess Rayleigh ratio, is plotted as a function of the droplet size at four different volume fraction of droplets. The microemulsion droplets, being small compared to the wavelength of the light, did not give rise to any angular dependence of the intensity. In agreement with earlier studies [29,30], the system exhibited a well-defined minimum, corresponding to the optical match point, around w_0 = 30. The scattered intensity decreased with a decrease in the volume fraction of droplets.

The apparent hydrodynamic radii, r_h^{app}, of the droplets were calculated through Eqs. (6) and (7), and Fig. 5 shows the variation of r_h^{app} with w_0. The size of the droplets should vary linearly with the molar ratio between water and AOT according to Eq. (8). However, this is only true for monodisperse droplets, and the sigmoidal shape of the curve around the match point may be explained by the polydispersity of the microemulsion droplets, as has been shown previously [29]. The decrease of r_h^{app} upon dilution has also been observed earlier [29], and the origin of this trend has been explained in detail by Yan and Clarke and Ricka and coworkers [45,46]. In

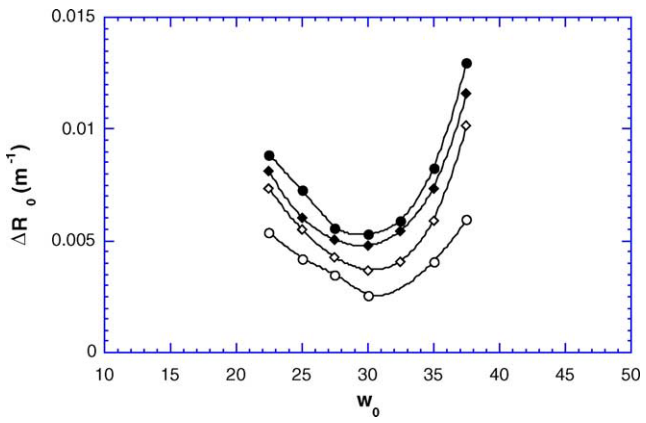

Fig. 4. Variation of absolute intensity with droplet size (w_0) in AOT/water/isooctane oil-continuous microemulsions at droplet volume fractions of 0.20 (filled circles), 0.15 (filled diamonds), 0.10 (open diamonds), and 0.05 (open circles). Lines are to guide the eye.

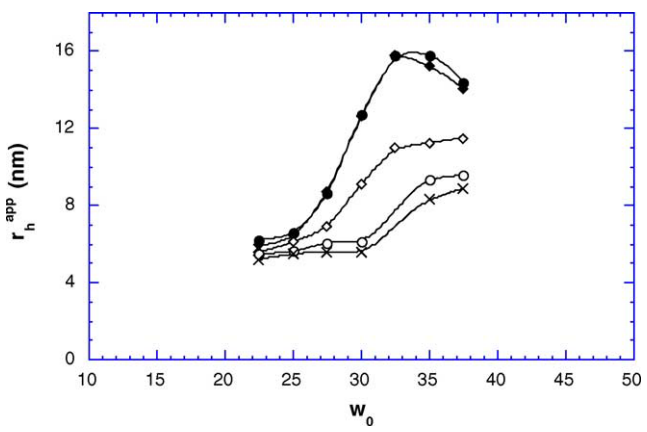

Fig. 5. Apparent hydrodynamic radii vs. droplet size (w_0) in AOT/water/isooctane oil-continuous microemulsions at droplet volume fractions of 0.20 (filled circles), 0.15 (filled diamonds), 0.10 (open diamonds), and 0.05 (open circles), and at infinite dilution (crosses). Lines are to guide the eye.

brief, the dynamic structure factor can be analyzed in terms of contributions from collective and self diffusion of the particles, and at the optical match point, the contribution from self diffusion dominates. The observed concentration dependence in Fig. 5 then follows from the fact that the self diffusion coefficient (as opposed to the collective diffusion coefficient) of particles decreases with increasing particle concentration. By linear extrapolation of the concentration dependences of the diffusion coefficients we have obtained the hydrodynamic radii at infinite dilution for the various particle sizes, and these results are also plotted in Fig. 5.

The CONTIN analysis of the DLS data gave a single well-defined peak in all mixtures of AOT/water/isooctane (Fig. 6).

3.4. Light scattering from PDMA in isooctane

Fig. 7a shows the SLS data for the unsubstituted PDMA in isooctane. The absolute scattered intensity is plotted as a function of the polymer concentration. Note that all scattered intensities plotted in Fig. 7 are higher than those recorded for any of the oil-continuous microemulsions in Fig. 4. The apparent weight-average molar mass, M_{app}, and the radius of gyration, r_g, of P_0 in isooctane calculated from Eqs. (3) and (5) are given in Table 1 above. The apparent radius of gyration, as obtained from Eq. (5), decreased with increasing polymer concentration, and the value 24 nm corresponds to the value at infinite dilution. The second virial coefficient, obtained from the slope of $Kc/\Delta R_\theta$ versus the polymer concentration, was positive.

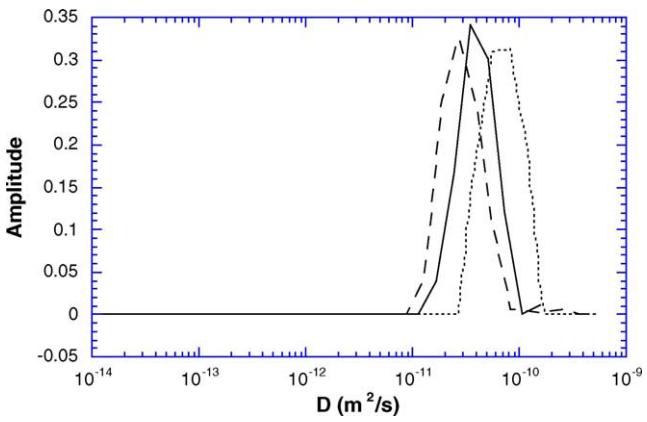

Fig. 6. Distribution of diffusion coefficients calculated by CONTIN in mixtures of AOT/water/isooctane for ϕ_d = 0.20 and w_0 = 22.5 (dotted line) or w_0 = 37.5 (dashed line), and in P_0/isooctane at c_{pol} = 7.50 g/dm^3 (solid line).

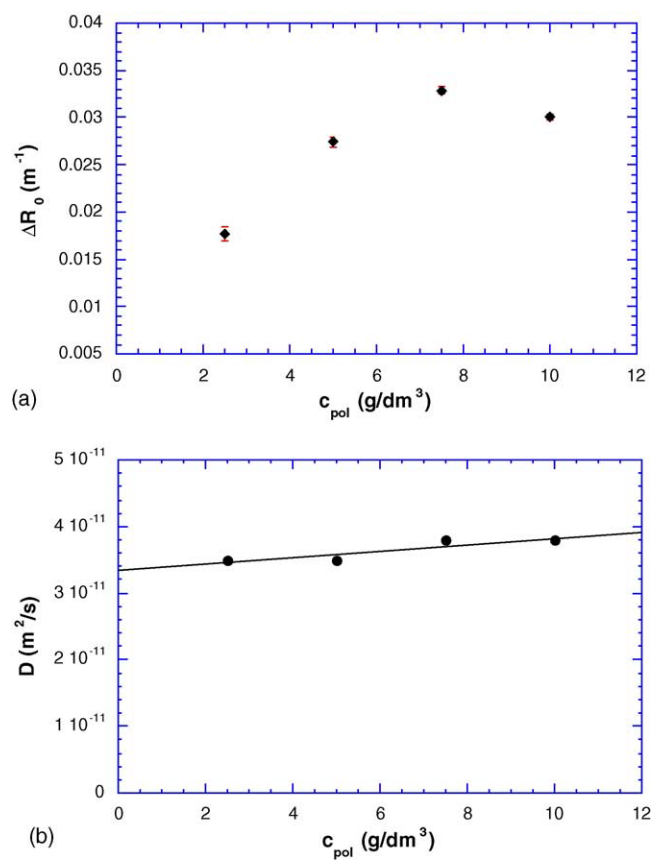

Fig. 7. (a) Absolute intensities vs. concentration of P_0 in isooctane. (b) Diffusion coefficient vs. concentration of P_0 in isooctane. The solid line shows the extrapolation to zero polymer concentration.

The CONTIN analyses of the DLS data consistently showed one population of diffusion coefficients for P_0; a sample distribution is shown together with the similar analyses for two pure microemulsions in Fig. 6. The diffusion coefficient increased slightly with increasing concentration, as seen in Fig. 7b. This is consistent with an effectively repulsive pair interaction (good solvent). The hydrodynamic radius calculated from D_0 by Eq. (7) is 14 nm, in good agreement with the value 12 nm estimated from the intrinsic viscosity (Table 1). The ratio between r_g and r_h (from light scattering), thus equals 1.7 for P_0 in isooctane. This may be compared with the theoretical value 1.29 for a Gaussian chain [47,48].

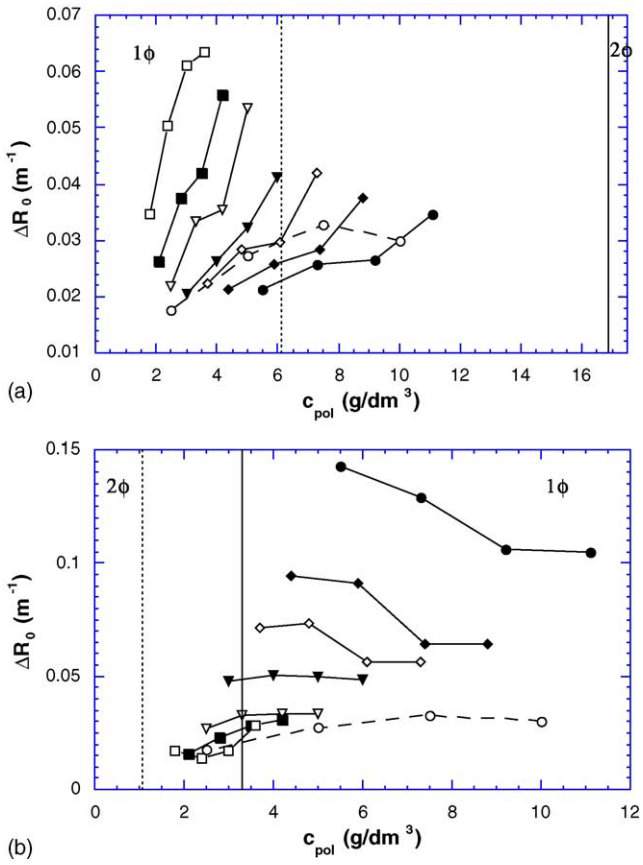

Fig. 8. Absolute intensities in mixtures of (a) P_0/droplet/isooctane, and (b) P_2/droplet/isooctane vs. polymer concentration. For comparison data for P_0 in isooctane (open circles) are also given. The phase boundaries between the one phase and two-phase areas are indicated for mixtures with the two extreme droplet sizes w_0 = 22.5 (solid lines) and w_0 = 37.5 (dotted lines). Symbols refer to w_0 = 22.5 (filled circles), w_0 = 25.0 (filled diamonds), w_0 = 27.5 (open diamonds), w_0 = 30.0 (filled triangles), w_0 = 32.5 (open triangles), w_0 = 35.0 (filled squares), and w_0 = 37.5 (open squares).

3.5. SLS from polymer-containing microemulsions

The variation of the absolute scattered intensity with the polymer concentration in P_0- and P_2-containing microemulsions is shown together with ΔR_0 of P_0 in isooctane in Fig. 8. (We recall that the number of droplets per polymer molecule was the same in all microemulsion samples.) The scattered intensity showed an angular dependence and the plotted values are extrapolations to $q = 0$. The scattered intensities from the polymer-containing microemulsions were much higher than those from the corresponding polymer-free microemulsions (see Fig. 4). In most of the systems, they were also higher than for the comparable solutions of P_0 in isooctane.

The variation in the scattered intensity with the polymer concentration looks very different for the two different polymers. In P_0-containing microemulsions (Fig. 8a) the scattered intensity increases with increasing polymer concentration for all samples, and the dependence becomes markedly stronger as the droplet size increases. The absolute value of ΔR_0, thus increases strongly with increasing droplet size. For the P_2-containing microemulsions, on the other hand, ΔR_0 increases very strongly with decreasing droplet size; see Fig. 8b. Moreover, the polymer concentration dependence is different for large and small droplets. For smaller droplets, the absolute intensity increases with decreasing polymer concentration. A cross-over occurs around w_0 = 30; for larger droplets, ΔR_0 increases with increasing polymer concentration, and the results are fairly similar to those for P_0 in isooctane.

Qualitatively, the scattering data can be understood from considering the particular phase behavior of the two systems. The phase boundaries for the extreme droplet sizes investigated in the present study (w_0 = 22.5 and 37.5) are indicated in Fig. 8, and we see that for both polymers, the large increase in scattering occurs as the phase boundary is approached. We recall from Fig. 2, where the compositions of the samples investigated by light scattering are indicated, that the mixtures with P_0 phase separates at higher concentrations, while in the P_2 system the polymer cannot be completely solubilized at lower concentrations. As phase separation is approached, we find an increase in the scattered light intensity due to concentration fluctuations. In the P_0 system, phase separation is favoured by larger droplets, while in the P_2 system, the larger droplets are more efficient in solubilizing the hydrophilic side chains, hence increasing the solubility of the polymer. More quantitatively, ΔR_0 depends on the details of droplet–droplet, droplet–polymer and polymer–polymer interactions as a sum of partial structure factors. Far away from phase separation we also observe overall repulsive interactions in the mixture of the P_0 polymer and small droplets as seen by the fact that the scattered intensity of the mixture is slightly smaller than the sum of droplets and polymer alone. The binodal line in the P_0 mixtures contains a critical point, and as phase separation is approached the magnitude of the scattered intensity contains information on the distance from the critical point. A comparison between the different droplet sizes indicates that we are closer to the critical point in the case of the larger droplets. In the case of the P_2 polymer the phase separation involves essentially polymer precipitation and the binodal line is not expected to contain a critical point. The high-scattered intensity observed for mixtures with small droplets indicates the aggregation of polymer molecules, possibly involving the hydrophilic side chains, as the these are not well solubilized by the small droplets. At present we cannot exclude the possibility that this also involves a splitting of the droplet population into larger and smaller droplets where the larger droplets solubilize the hydrophilic side chains.

3.6. DLS from polymer-containing microemulsions

Fig. 9 compares representative distributions of diffusion coefficients, obtained from CONTIN analyses, for polymer-containing and polymer-free microemulsions. Both polymer-containing microemulsions give bimodal distributions, with one peak closely corresponding to the single peak from the polymer-free microemulsion. There can be little doubt that this peak corresponds to microemulsion droplets. Thus, the

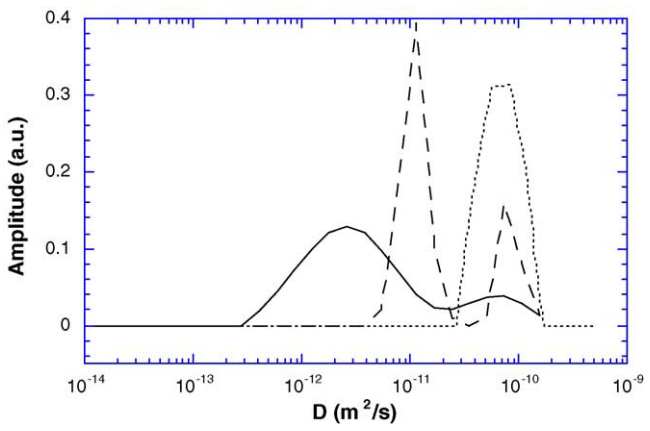

Fig. 9. Distribution of diffusion coefficients calculated by CONTIN in mixtures of droplets/isooctane (dotted line), P_0/droplet/isooctane (dashed line), and P_2/droplet/isooctane (solid line) at $\phi_d = 0.20$, $w_0 = 22.5$. The polymer concentration in the latter two mixtures was 11.1 g/dm^3.

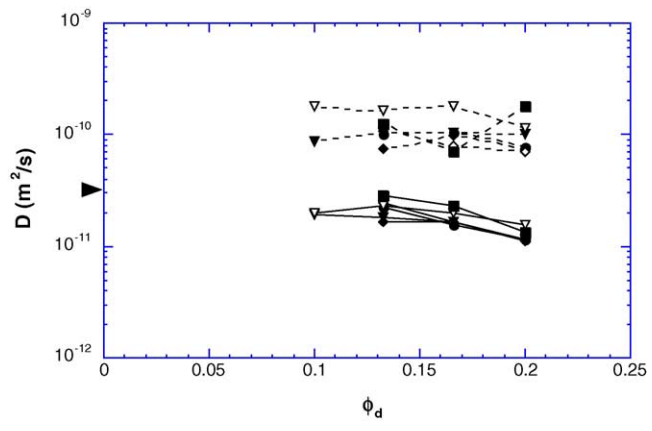

Fig. 10. Diffusion coefficients of droplets (dotted lines) and polymer molecules (solid line) vs. volume fraction of droplets in mixtures of P_0/droplet/isooctane. Arrow indicates diffusion coefficient for P_0 at infinite dilution in isooctane (from Fig. 7b. 7b. Symbols refer to $w_0 = 22.5$ (filled circles), $w_0 = 25.0$ (filled diamonds), $w_0 = 27.5$ (open diamonds), $w_0 = 30.0$ (filled triangles), $w_0 = 32.5$ (open triangles), and $w_0 = 35.0$ (filled squares).

DLS data confirm our previous indirect conclusion, from NMR self-diffusion measurements, that the mixtures with the graft copolymer contain a significant fraction of droplets that are not bound to the polymer. The additional peak in the distributions for the mixtures corresponds to a more slowly diffusing component, i.e., the polymer. The polymer peak is broader, and has a slower mean diffusion coefficient, for the samples containing the graft copolymer. This is consistent with the formation of polydisperse polymer–droplet aggregates.

Similar CONTIN analyses were made for all polymer/microemulsion mixtures (not shown), and they showed the following trends. In samples with polymer P_0 the resolved droplet peak disappeared in certain mixtures. At constant w_0, the two peaks merged into one with increasing dilution. This effect is probably due to limitations in the ability of the CONTIN analysis to resolve the two peaks at increasing dilution. The CONTIN distributions of the P_2-containing microemulsions were less "clean", as compared to the results for the P_0-containing microemulsions; there was a larger variation between distributions obtained at different angles, and the free droplet peak was less well resolved from the polymer peak. In both types of mixture, the two peaks merged when w_0 was increased.

Figs. 10 and 11 show the concentration dependences of the diffusion coefficients for all polymer-containing microemulsions that gave separated droplet and polymer peaks. On the whole, the measured diffusion coefficient of each type of object, i.e., a free droplet, a free polymer (in the P_0-containing samples), or a polymer–droplet aggregate (in the P_2-containing samples) is rather insensitive to variations in w_0 or in the overall concentration, but there are nevertheless, some significant trends. The scatter in the data for the droplet diffusion obscures possible variations with w_0 or concentration for a given type of polymer. The mean diffusion for the droplets in the P_2-containing samples is, however, slower than in the mixtures with P_0. In both systems, the polymer diffusion decreases significantly with increasing droplet concentration. Moreover, the data for different droplet sizes more or less collapse on the same lines when the droplet volume fraction is used as the concentration variable. Such a collapse did not occur when the data were, instead, plotted against the polymer concentration (recall that both the droplet and the polymer concentrations were varied in the dilution series studied). This indicates that the weak concentration effects are indeed due to the variations in the volume fraction of droplets.

We conclude this section with calculations of apparent hydrodynamic radii of the polymers, using Eq. (7) and the D values obtained at the maxima of the polymer peaks of the CONTIN analyses. Calculations were only made for the cases shown in Figs. 10 and 11, where the polymer peak was well resolved. These calculations require values for the viscosities of the dispersion medium. Since, the droplets are smaller than

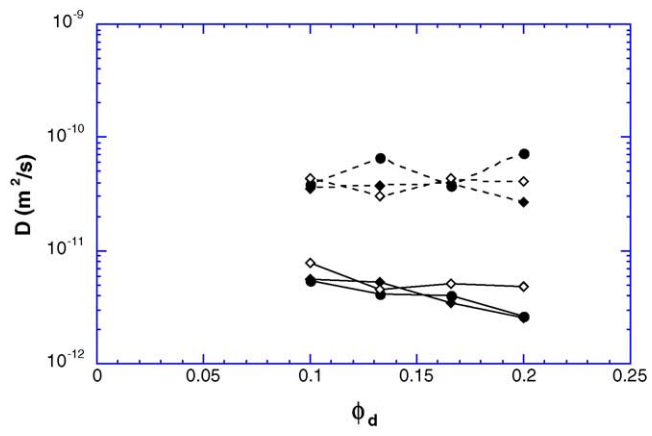

Fig. 11. Diffusion coefficients of droplets (dotted lines) and polymer molecules (solid line) vs. volume fraction of droplets in mixtures of P_2/droplet/isooctane. Symbols refer to $w_0 = 22.5$ (filled circles), $w_0 = 25.0$ (filled diamonds), $w_0 = 27.5$ (open diamonds).

the radius of gyration of the polymers we have used the approximation that the effective viscosity seen by the polymer is given by the viscosity of the polymer-free microemulsions. In this way, we obtain a value of r_h^{app} = 15 nm for P_0, independently of the concentration or droplet size in the measurable range. This value is very close to the hydrodynamic radius of 14 nm obtained for P_0 in pure isooctane and supports the notion that P_0 appears as a flexible chain in the microemulsion with the same dimensions as in pure isooctane. Moreover, it suggests that the variation in polymer diffusion coefficients in Fig. 10 is due to the increasing viscosity of the microemulsion at higher droplet concentrations.

For P_2 system where we have association between droplets and polymer the situation is more complex. We obtain r_h^{app} values in the range 30–64 nm. Weak trends suggest that r_h^{app} is larger for at high concentrations and small droplet sizes. We have in a previous study performed NMR self-diffusion measurements of the graft copolymer in AOT/water/cyclohexane oil-continuous microemulsions [6]. There it was found that the size of the polymer–droplet aggregates decreased when the polymer concentration was decreased at a constant droplet concentration and (for sufficiently dilute systems) when the droplet concentration was decreased at constant polymer concentration. Sizes similar to those obtained here emerged from the NMR study for comparable mixtures. For instance, r_h of P_2, calculated from the polymer self-diffusion coefficient measured by PFG-NMR, was 60 nm in AOT/water/cyclohexane oil-continuous microemulsion with w_0 = 23, ϕ_d = 0.17 and c_{pol} = 9.4 g/dm^3.

4. Conclusions

In this study, we have regarded the microemulsion droplet as a pseudo-component in polymer/droplet/isooctane mixtures. We have obtained information on the polymer–droplet interactions from the macroscopic phase behavior of the mixtures as well as from the microscopic structure and dynamics in single-phase solutions, as obtained by light scattering. By studying mixtures, where the droplets were nearly optically matched to the solvent, information on the polymer component could be obtained in solutions where the polymer concentration was much lower than the droplet concentration. The results show that the parent PDMA polymer and the PDMA-g-PEO graft copolymer behave quite differently in oil-continuous microemulsions. The phase behavior of both types of mixture show strong similarities with the analogous water-continuous mixtures, where either water-soluble hydrophilic homopolymers, or hydrophobically modified polymers, are mixed with micelle-forming surfactants.

The parent PDMA polymer is miscible with the microemulsion droplets in the dilute concentration range, but a segregative phase separation occurs at high volume factions of droplets. The polymer–droplet interaction is repulsive and the polymer dissolves in the oil-continuous phase without associating to the droplets. The PDMA/droplet segregation is stronger for larger droplets. All data consistently indicate that PDMA behaves as a flexible chain both in the pure oil and in the microemulsions. The graft copolymer–droplet interaction is attractive, and PDMA-g-PEO dissolves in the microemulsion with the backbone in the oil continuous phase and the side chains anchored into the water droplets. Dynamic light scattering data show that large polymer–droplet aggregates, with a broad size distribution, are formed. DLS data also confirm the existence of free droplets, which was concluded previously from indirect NMR self-diffusion evidence. Phase separation occurs when the concentration of droplets becomes sufficiently low, and a large concentration of droplets is required to solubilize even small amounts of PDMA-g-PEO. The mass concentration of droplets required to solubilize the graft copolymer increases with increasing droplet size, but the overall number of droplets required to dissolve the graft copolymer is lower for larger droplets. The stoichiometry of the polymer–droplet aggregates is changed when the overall side chain/droplet ratio varies.

Acknowledgments

We thank Karin Schillén for valuable discussions concerning the light scattering results and Cornelia Sommer for help with light scattering measurements. This work was supported by a grant from the Centre for Amphiphilic Polymers from Renewable Resources at Lund University (CAP).

References

[1] J.C.T. Kwak, Polymer–Surfactant Systems, Marcel Dekker, New York, 1998.
[2] L. Piculell, K. Thuresson, B. Lindman, Polym. Adv. Technol. 12 (2001) 44–69.
[3] A. Holmberg, L. Piculell, B. Wesslén, J. Phys. Chem. 100 (1996) 462–464.
[4] J. Eastoe, B.H. Robinson, D.C. Steytler, D. Thorn-Leeson, Adv. Colloid Interface Sci. 36 (1991) 1–31.
[5] A. Holmberg, P. Hansson, L. Piculell, P. Linse, J. Phys. Chem. 103 (1999) 10807–10815.
[6] A. Holmberg, L. Piculell, M. Nydén, J. Phys. Chem. B 106 (2002) 2533–2544.
[7] C. Quellet, H-F. Eicke, G. Xu, Hauger Y, Macromolecules 23 (1990) 3347–3352.
[8] R.P.W. Struis, H.-F. Eicke, J. Phys. Chem. 95 (1991) 5989.
[9] U. Zölzer, H-F. Eicke, J. Phys. II France 2 (1992) 2207–2219.
[10] M. Odenwald, H-F. Eicke, W. Meier, Macromolecules 28 (1995) 5069–5074.
[11] R.A. Gelman, International Dissolving Pulps Conference, TAPPI Proc., 1987, 159–165.
[12] J.D. Abdulkadir, A.C. Steiner, Macromolecules 23 (1990) 251–255.
[13] I. Iliopoulos, T.K. Wang, R. Audebert, Langmuir 7 (1991) 617–619.
[14] R. Tanaka, J. Meadows, P.A. Williams, G.O. Phillips, Macromolecules 25 (1992) 1304–1310.
[15] B. Magny, I. Iliopoulos, R. Audebert, L. Piculell, B. Lindman, Progr. Colloid Polym. Sci. 89 (1992) 118–121.
[16] E.D. Goddard, P.S. Leung, Colloids Surf. 65 (1992) 211–219.

[17] B. Magny, I. Iliopoulos, R. Zana, R. Audebert, Langmuir 10 (1994) 3180–3187.
[18] S. Abrahmsén-Alami, P. Stilbs, J. Phys. Chem. 98 (1994) 6359–6367.
[19] T. Annable, R. Buscall, R. Ettelaie, P. Shepherd, D. Whittlestone, Langmuir 10 (1994) 1060–1070.
[20] K. Persson, G. Wang, G. Olofsson, J. Chem. Soc. Faraday Trans. 90 (1994) 3555.
[21] U. Kästner, H. Hoffmann, R. Dönges, R. Ehrler, Colloids Surf. A 82 (1994) 279–297.
[22] I. Iliopoulos, U. Olsson, J. Phys. Chem. 98 (1994) 1500–1505.
[23] A. Sarrazin-Cartalas, I. Iliopoulos, R. Audebert, U. Olsson, Langmuir 10 (1994) 1421–1426.
[24] B. Nyström, K. Thuresson, B. Lindman, Langmuir 11 (1995) 1994–2002.
[25] L. Piculell, F. Guillemet, K. Thuresson, V. Shubin, O. Ericsson, Adv. Colloid Interface Sci. 63 (1996) 1–21.
[26] K. Thuresson, B. Lindman, B. Nyström, J. Phys. Chem. B 101 (1997) 6450–6459.
[27] E. Jiménez-Regalado, J. Selb, F. Candau, Langmuir 16 (2000) 8611–8621.
[28] L. Piculell, M. Egermayer, J. Sjöström, Langmuir 19 (2003) 3643–3649.
[29] M. Zulauf, H.F. Eicke, J. Phys. Chem. 83 (1979) 480–486.
[30] S. Christ, P. Schurtenberger, J. Phys. Chem. 98 (1994) 12708–12714.
[31] C. González-Blanco, M.M. Velázquez, Langmuir 13 (1997) 6095–6100.
[32] B. Wesslén, K.B. Wesslén, J. Polym. Sci. A: Polym. Chem. 27 (1989) 3915–3926.
[33] P. Rempp, E. Franta, J.-E. Herz, Adv. Polym. Sci. 86 (1988) 168–170.
[34] P. Schurtenberger, R.C. Augusteyn, Biopolymers 31 (1991) 1229.
[35] R.J. Hunter, Introduction to Modern Colloid Science., Oxford, Oxford University Press, 1993.
[36] D.E. Koppel, J. Chem. Phys. 57 (1972) 4814–4820.
[37] R.M. Johnsen, W. Brown, S.E. in: Harding, D.B. Sattelle, Bloomfield VA Laser Light Scattering in Biochemistry, Royal Society of Chemistry, Cambridge, 1992.
[38] J. Ricka, M. Borkovec, U. Hofmeier, J. Chem. Phys. 12 (1991) 8503–8509.
[39] P. Schurtenberger, in: W. Brown (Ed.), Light Scattering Principles and Development, Oxford University Press, Oxford, 1996, pp. 293–326.
[40] I.D. Robb, P.A. Williams, P. Warren, R. Tanaka, J. Chem. Soc., Faraday Trans. 91 (1995) 3901–3906.
[41] L. Piculell, K. Bergfeldt, S. Gerdes, J. Phys. Chem. 100 (1996).
[42] E.D. Goddard, J. Colloid Interface Sci. 152 (1992) 578–581.
[43] F. Guillemet, L. Piculell, J. Phys. Chem. 99 (1995) 9201–9209.
[44] A.K. Morén, A. Khan, Langmuir 14 (1998) 6818–6826.
[45] Y.D. Yan, J.H.R. Clarke, J. Chem. Phys. 93 (1990) 4501–4509.
[46] J. Ricka, M. Borkovec, U. Hofmeier, H.-F. Eicke, Europhys. lett. 11 (1990) 379–385.
[47] W. Burchard, M. Schmidt, W.H. Stockmayer, Macromolecules 13 (1980) 1265–1272.
[48] K. Schillén, A. Yekta, N. Shaoru, Farinha JPS, M.A. Winnik, J. Phys. Chem. 103 (1999) 9090–9103.